Contrasting Land-Uses Affect Chemical Composition of Organic Matter in Tropical Soils: A Case Study via Os Staining and FTIR

Maoz Dor[1]*, Ricardo de Oliveira Bordonal[2], Andrey K. Guber[1], Mark L. Rivers[3] and Alexandra N. Kravchenko[1]

1. Department of Plant, Soil and Microbial Sciences, Michigan State University, East Lansing, MI, USA
2. Brazilian Bioenewables National Laboratory, Brazilian Center for Research in Energy and Materials (LNBR/CNPEM), Rua Giuseppe Máximo Scolfaro 10000, Campinas, SP 13083-100, Brazil.
3. Department of Geophysical Sciences and Center for Advanced Radiation Sources, the University of Chicago

* Corresponding author dormaoz@msu.edu

Abstract

Particulate organic matter (POM) is a significant component of soil organic carbon (SOC), particularly in tropical soils, where it often serves as a primary precursor for the formation of mineral-associated organic matter (MAOM). This study investigates the impact of contrasting land-use practices on composition of POM in tropical soils. Using dual-energy X-ray microtomography approach with osmium tetroxide (OsO_4) staining, we visualized and quantified two types of POM: root-derived and pyrogenic (pyC), in soils of three land-use systems: crop succession, integrated crop-livestock (ICL), and managed pasture. Fourier transform infrared (FTIR) spectroscopy was employed to analyze the chemical composition of the two POM types. Results showed that land-use practices significantly influenced pyC chemical composition and Os staining efficiency, with ICL exhibiting the highest concentration of staining Os, followed by pasture and crop succession. Root-derived POM showed no significant differences in Os staining across land uses. FTIR analysis revealed distinct chemical signatures among land uses, with ICL demonstrating lower aromatic-to-aliphatic carbon ratios in pyC, suggesting enrichment by plant-derived aliphatic materials. These findings can be attributed to intensive decomposition of fresh organic inputs during crop-pasture rotations in ICL system, providing new insights into the mechanisms through which POM of pyrogenic origin may contribute to SOC accrual and protection in tropical soils under different management practices.

Key words: x-ray tomography, soil organic carbon, particulate organic matter, pyrogenic carbon, Os staining, IR spectroscopy

Abbreviation: Integrated crop-livestock, ICL; X-ray microtomography, μCT; soil organic carbon, SOC; Particulate organic matter, POM; pyrogenic carbon, pyC

Introduction

Adoption of agriculture led to major depletions of soil carbon, which combined with other human activities, has significantly altered the global carbon balance. Soil organic carbon (SOC) is the largest terrestrial carbon reservoir and a crucial climate regulator (Bossio et al., 2020; Sanderman et al., 2017) influencing numerous soil processes essential for soil health and functioning, including nutrient cycling, regulation of physical and chemical properties, and microbial activities (Kögel-Knabner et al., 2022; Lehmann and Kleber, 2015). The dynamic nature of SOC, which is heavily influenced by land use practices and soil management, means it can act as both a source and a sink for the atmospheric carbon (Bossio et al., 2020; Lal, 2004).

Advancements in X-ray microtomography (μCT) have enabled researchers to overcome soil opacity, image and quantify soil structure, addressing issues such as fluid flow, soil stability, root growth, and carbon dynamics (Dor et al., 2019; Kravchenko et al., 2019; Schlüter et al., 2022, 2014). Peth et al. (2014) introduced a novel method to visualize SOC using synchrotron μCT and osmium tetroxide (OsO_4), which bonds with organic compounds. Yet, despite the opportunities this method presents to explore SOC dynamics and mechanisms, only few studies have used so far (Arai et al., 2019; Rawlins et al., 2016; Schlüter et al., 2022; Zheng et al., 2020). The limited adoption likely stems from the challenges inherent to the approach. Those include technical difficulties in getting access to synchrotron-based monochromatic scanning and the handling of extremely toxic osmium tetroxide. But also among the potential restrictions is high micro-scale variability in osmium (Os) staining performance due to (1) the spatial complexity and variance of intact soil samples which often results in low signal-to-noise images; (2) extreme heterogeneity of organic compounds constituting SOC with myriad potential Os bonding sites, potentially leading to non-preferential staining resulting in inconsistent or uneven staining patterns; (3) limitations in Os diffusion to SOC staining sites through highly variable and tortuous soil matrix. Better

understanding and quantification of the limits of Os approach can improve its application, enabling better quantitative analysis of SOC processing while studying soil in its intact state.

Particulate organic matter carbon (POM-C) represents a substantial fraction of SOC, typically accounting for 10-30% of total SOC and >50% in organic soils (Angst et al., 2023; Cotrufo et al., 2019). In tropical soils, POM plays a particularly crucial role, often accumulating faster than mineral-associated organic matter (MAOM) and serving as its direct precursor (Yu et al., 2022). Previous studies using Os staining found POM to be particularly suitable for labeling and visualization (Arai et al., 2019; Maenhout et al., 2021; Rawlins et al., 2016; Schlüter et al., 2022; Zheng et al., 2020). The reactivity of organic components with OsO_4 is due to its reaction with alkenes to form cyclic esters (Collin and Griffith, 1974). For instance, OsO_4 reacts with the olefinic sites of unsaturated fatty acids to form mono- and di-esters, as seen in lipids and phospholipids (Belazi et al., 2009). Lewis bases (e.g., tertiary amines) accelerate this reaction by forming complexes that add more rapidly to the alkene, such as complexes involving Os mono-esters and electron-donor ligands from amino acids (Belazi et al., 2009). However, POM can originate from diverse sources, resulting in a wide range of organic carbon compounds and species. This diversity makes consistent soil staining challenging. Consequently, staining effectiveness and response in soil samples can vary considerably, potentially limiting the consistent implementation of this method and affecting the interpretation of results.

The goal of this study was to explore POM in the soils subjected long-term differences in land use and management, namely, row crop succession, integrated crop-livestock, and managed pasture systems using Os staining and FTIR analysis, with expectation that such differences can affect POM composition and origin. Integrated crop-livestock and pasture systems, considered nature-based solutions for enhancing SOC accrual in Brazilian tropical soils, while crop succession serves as a comparison to the current prevailing system (Monteiro et al., 2024). The crop-livestock and pasture systems integrate monoculture grass and cattle grazing, contributing to increased carbon-rich organic residues above and below ground, thus promoting C accrual (Bieluczyk et al., 2020; Brewer and Gaudin, 2020; Carvalho et al., 2010). We hypothesized that POM of recent plant origin, e.g., root residues, will differ among the studied systems reflecting differences in the prevailing vegetation. Historical burning practices in these fields resulted in substantial quantities of pyrogenic POM (Nascimento et al., 2020; Roscoe et al., 2000). We hypothesized that chemical

characteristics of POM of pyrogenic origin have been defined by the historic burning and will not respond to current changes in land use. Moreover, since pyrolysis increases the aromaticity of organic materials (Chen et al., 2024; Collard and Blin, 2014), and aromatic compounds have fewer bonding sites for Os, we anticipated that pyrogenic POM would be weakly stained by Os and thus poorly visible on X-ray μCT scans, in contrast to root-derived POM.

Materials and Methods

Experimental site

Samples were collected from a long-term experiment at the Brazilian Agricultural Research Corporation (EMBRAPA Agrossilvipastoril) experimental station in Sinop, Mato Grosso, Brazil (11° 51'S – 55° 35'W, 370 m altitude). The climate is tropical savanna with a mean annual temperature of 25.6 °C and rainfall of 1974 mm. The soil is a Typical Hapludox clay (56% clay, 16% silt, 28% sand). The experiment, established in 2011, used a complete randomized block design with three land use treatments and four replicates (blocks), each plot covering 2 ha. The treatments were: (1) Crop succession: soybean (*Glycine max* L.) and corn (*Zea mays*) under no-till rotation (no-till); (2) Integrated crop-livestock (ICL): Four-year cycle alternating between crop succession (two years) and palisade grass (*Urochloa brizantha*) monoculture for cattle grazing (two years); (3) Well-managed pasture (Pasture): Continuous palisade grass for cattle grazing. The experiment was established in regions historically used for pasture, where fire is a common management practice and accidental burns have been reported prior to the installment of the experiment (Roscoe et al., 2000).

Twelve intact soil cores (⌀=5cm, h=5cm) were collected at 0-10 cm depth in 2021, one per replicated plot, and stored at 4°C until further analysis.

Sample preparation and Os staining

For organic fragment imaging and spectroscopy, soils were air-dried and sieved (2 mm). Roots and pyrogenic carbon (pyC) fragments were randomly selected and separated from the air-dried soil. For X-ray computed tomography (μCT) imaging, the fragments were packed in custom printed cylinders (⌀=0.8cm, h=1cm) with three separate sub-compartments designed to facilitate easy identification of the individual fragments and for keeping track of them during image analysis. For each land use we had six root fragments and six pyC fragments that were embedded within

fine pure quartz sand (⌀=150-400 µm, Acros Organics, Netherlands). The sand medium held the fragments in place, while enabling efficient gas diffusion through its pore space. This setting allowed us to examine the Os staining of the organic matter fragments within a pore system without the soil background noise.

Soil organic matter staining was performed using sodium tetraoxide (OsO_4) vapors. While in the past the staining was accomplished by allowing free diffusion of OsO_4 into the samples under atmospheric pressure (Maenhout et al., 2021; Peth et al., 2014; Schlüter et al., 2022; Zheng et al., 2020), in this study we employed the vacuum system to enhance staining efficiency by facilitating OsO_4 transport into pores. Samples were placed in a vacuum desiccator (-90 kPa) connected to a flask containing 10 mL of 2% OsO4 solution (Fig. 1a). After establishing vacuum, the valve to the OsO_4 was carefully opened, exposing sample surfaces to OsO_4 vapors for 48 hours. Samples were stored at room temperature before µCT analysis.

Dual energy X-ray tomography

This technique involves imaging samples twice with monochromatic µCT above and below the osmium K-edge, allowing the locations of stained organic materials to be determined from the differences between these images. X-ray tomography imaging was conducted at the GeoSoilEnviroCARS (GSECARS) BM-13D beamline of the Advanced Photon Source, Argonne National Laboratory, IL, USA. Sequential images were collected above (74.0 keV) and below (73.7 keV) the Os K-edge. Total of 720 projections were collected for each sample at 5.74 μm^3/voxel resolution (Fig. 1b-c). Raw images were preprocessed and reconstructed using GSECARS algorithms (Rivers, 2012).

To quantify Os content, pyrogenic carbon (pyC) and root-POM were segmented from above K-edge images using a deep-learning approach implemented with ORS Dragonfly (build 2022.1). A training set (<2% of image volume) was created by manual annotation, with pyC and root POM as foreground and the rest as background. The trained model was applied to the entire image, resulting in a binary image of pyC and root POM. This binary image was used to isolate intensity values for POM fragments in below and above Os K-edge images (Fig. 1d). Os concentration was calculated using the approach reported by Zheng et al. (2020) and the following equation:

$$Os = \frac{\mathrm{I_a} - I_b}{fr\Delta\mu\rho^{-1}} = 0.226 \times 10^{-3}(\mathrm{I_a} - I_b)$$

where Os is the Os concentration in image voxels (g·cm−3), $\mathrm{I_a}$ and I_b are the grayscale intensity values of above- and below K-edge images, respectively, r is the voxel resolution (5.74 μm), f is the conversion coefficient from 32-bit floating point to 16-bit integer (10^6), $\Delta\mu\rho^{-1}$ is the difference between the photon mass attenuation coefficients μ/ρ for above and below K-edge energies for Os (7.75 $cm^2\ g^{-1}$) (Hubbell and Seltzer, 1995).

Fourier transform infra-red spectroscopy (FTIR)

For FTIR spectroscopy, roots and pyC samples from the three land uses were randomly selected and separated, dried at 60°C for 3 days and ball-milled into powder. Fourier transformed infra-red (FTIR) spectra were collected on a Vertex 70 spectrometer (Bruker Scientific LLC, Bellerica, MD, USA) equipped with a PIKE Easy-Diff diffuse reflectance accessory (FTIR-DRIFT). Each spectrum represents an average of 60 scans per sample collected between 600-4000 cm^{-1} at a resolution of 4 cm^{-1}. Replicated spectra for each sample (n=4) were baseline corrected, normalized with the standard normal variate (SNV) method and smoothed (Savitsky-Goulay smoothing) (Fig. 1e). To identify differences originating from organic constituents among the samples, we integrated the area of three broad spectral ranges corresponding to different organic functional groups: 3000-2800 cm^{-1} corresponding to aliphatic C-H stretch, 1760-1550 cm^{-1} corresponding to C=O stretch, and 1550-1480 cm^{-1} corresponding to aromatic C=C stretch and/or carboxylate C-O asymmetric stretch and/or conjugated ketone C=O stretch (Margenot et al., 2023; Parikh et al., 2014; Yu et al., 2022). In addition, we used the three ratios of these representative functional groups to interpret the chemical composition of the two types of POM: aliphatic to carboxylic carbon, aromatic to aliphatic carbon, and aromatic to carboxylic carbon.

Statistical analysis

Differences across the land uses in Os staining concentration for the two types of POM were assessed using the linear mixed model approach implemented in the lme4 package in R (Bates et al., 2015) (version 4.2.2). The statistical model included the land use, POM type (i.e., pyC or roots), and their interaction as fixed effects, and the scanned cylinders as random effects. The normality assumption was assessed using normal probability plots of the residuals, and the

assumption of variance homogeneity was assessed by the residuals plots and the Levene's test. When the interactions between the land use and POM type were found to be statistically significant, we proceeded with examining the interactions using simple F-tests (aka slicing), which was then followed by all-pairwise comparisons among the means within each F-test slice.

We used the area under the curve calculated from FTIR spectra as the response in characterizing C functional groups. For these data, the statistical model included the fixed effects of the functional groups, land uses, POM types, and their interaction, and the replicates, nested within the land use and POM type, as random effect. To assess spectral differences and to visualize the variability in across the different land uses and POM types, principal component analysis (PCA), implemented in the factoMineR in R (Lê et al., 2008), was used to analyze the FTIR spectra. PCA reduces the dimensionality of the FTIR spectra data set comprising hundreds of absorbance intensities at different wavenumbers into principal components. We selected 5 principal components, which captured ~95% of the variance, for a linear discriminant analysis (LDA) which maximizes 'inter-group' variance over the 'intra-group' variance of the factors. The LDA was implemented in the MASS package in R (W. N. Venables and B. D. Ripley, 2002).

Results

Os staining efficiency differences among two types of POM

The Os staining results for the two types of POM from the different land uses are shown in Fig. 2. PyC POM had higher Os staining values compared to root POM (Table S1). Os concentrations of the root POM did not differ among the land uses, while Os concentrations of pyC were the highest in ICL, followed by Pasture and Crop succession.

FTIR spectroscopy analysis of the two types of POM

Principal Component Analysis (PCA) showed distinct clustering patterns among the three land uses, and the two types of POM (Fig. 3). The first two principal components accounted for 78.4% of the total variance, with the first principal component (Dim1) explaining 63.3% and the second principal component (Dim2) explaining 15.1%. The most distinct separation occurred between roots and pyC-POM along Dim1. PyC data points showed greater variance among land uses compared to roots, primarily along Dim1. Pasture roots were clearly separated from ICL and Crop succession roots. For pyC, the ICL land use fell between Crop succession and Pasture.

Further analysis of the two types of POM spectral data revealed distinct differences in chemical characteristics among the three land uses (Fig. 4, Table S2). Significant differences were observed between roots and pyC for all functional groups (Aliphatic C-H, Aromatic C=C, and C=O stretch) across all land uses, with distinct patterns of variation within each POM type. For the pyC, the C=O stretch functional group was lower in ICL compared to Crop succession and Pasture. In the roots, the C=O stretch was lower in Pasture than Crop succession and ICL. The Aromatic C=C group in pyC was highest in Crop succession, followed by Pasture, with ICL having the lowest values. In the roots, aromatic C=C values were uniformly low across all land uses. Aliphatic C-H in pyC was significantly higher in ICL, followed by Crop succession and Pasture. In the roots, ICL had the highest aliphatic C-H, followed by Crop succession and Pasture. Across all land uses, pyC exhibited higher aromatic C=C and C=O stretching than roots, while roots demonstrated higher aliphatic C-H stretching compared to pyC.

Fig. 5 illustrates the effects of different land uses on C functional group ratios in pyC and roots. Significant differences between the two POM types were observed across all land uses and functional group ratios. The aliphatic/carboxylic C ratio in pyC was highest in ICL, significantly differing from other land uses, while in roots, it was significantly lower in Crop succession compared to ICL and Pasture. The aromatic/aliphatic C ratio in pyC was significantly higher in Crop succession and Pasture compared to ICL. In roots, this ratio was highest in Pasture, followed by Crop succession, and lowest in ICL. The aromatic/carboxylic C ratio in pyC was higher for Crop succession, with no significant differences between ICL and Pasture. In roots, this ratio was highest in Pasture, followed by Crop succession and ICL.

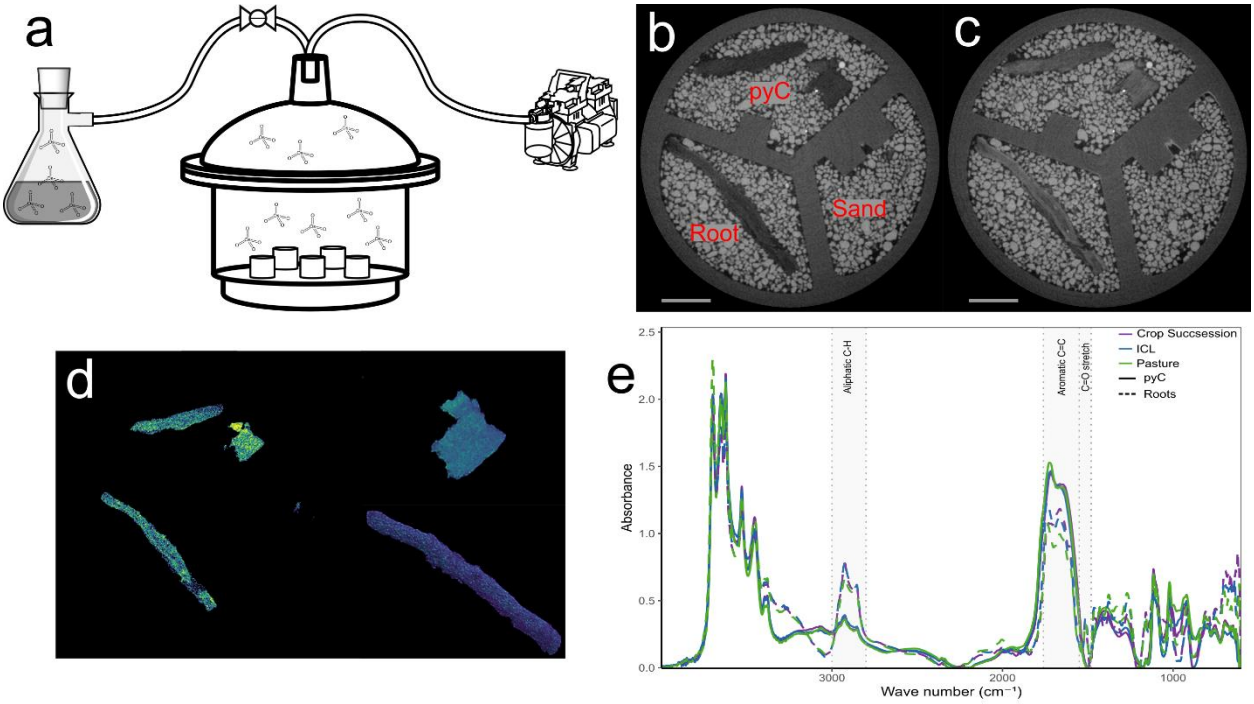

Fig. 1 Workflow for Os staining and FTIR spectroscopy for the two types of POM. Diagram showing the vacuum set up used for improved and consistent Os staining (a). µCT image showing the two types of POM fragments within the sand porous media scanned below (b) and above (c) the Os K-edge; scale bar is 1.5 mm. Os concentration derived from the above-below K-edge images (d). Baseline-corrected FTIR spectra of each POM type across the different land uses (e). Gray-shaded regions indicate the wavenumber ranges used for integrating spectral features to assign functional groups.

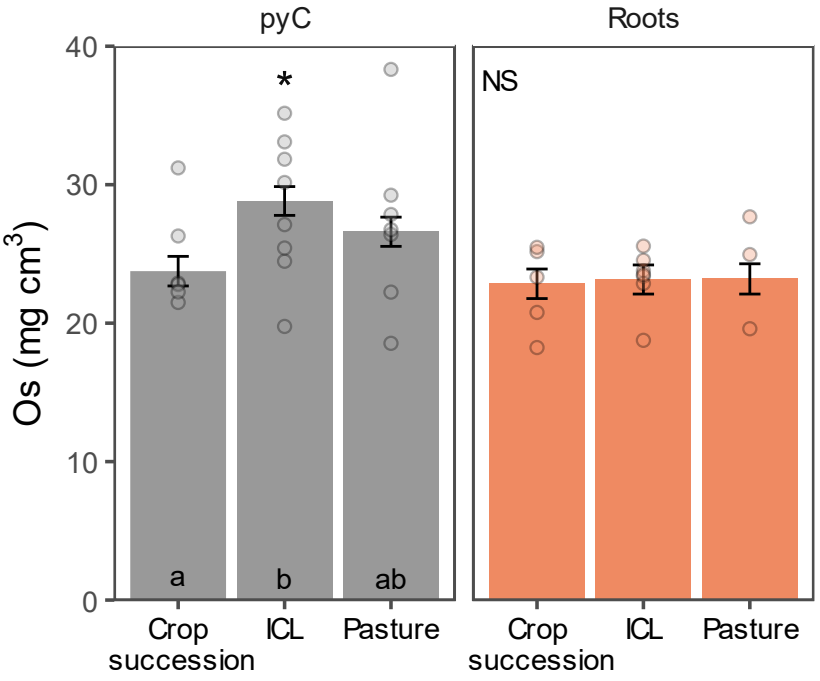

Fig. 2 Os staining for the different types of POM in the different land uses. Shown are means and standard errors for the means, letters indicate significant differences among land uses and * mark significant differences between pyC and roots within a land use ($p<0.05$).

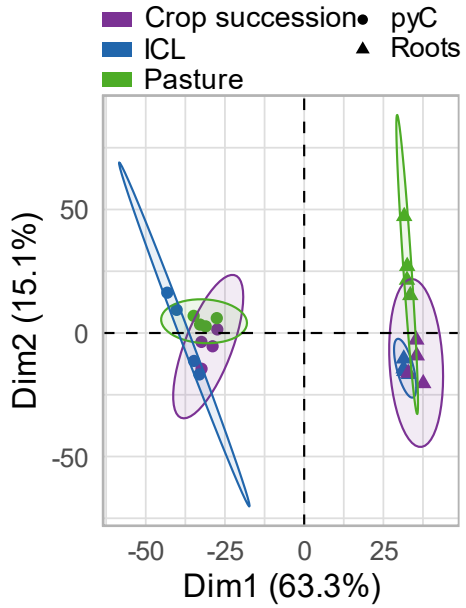

Fig. 3 Principal component analysis of FTIR spectra visualizing the variability of spectral data in the two types of POM of the studied land uses. Ellipses represent 95% confidence level around centroid of different groups.

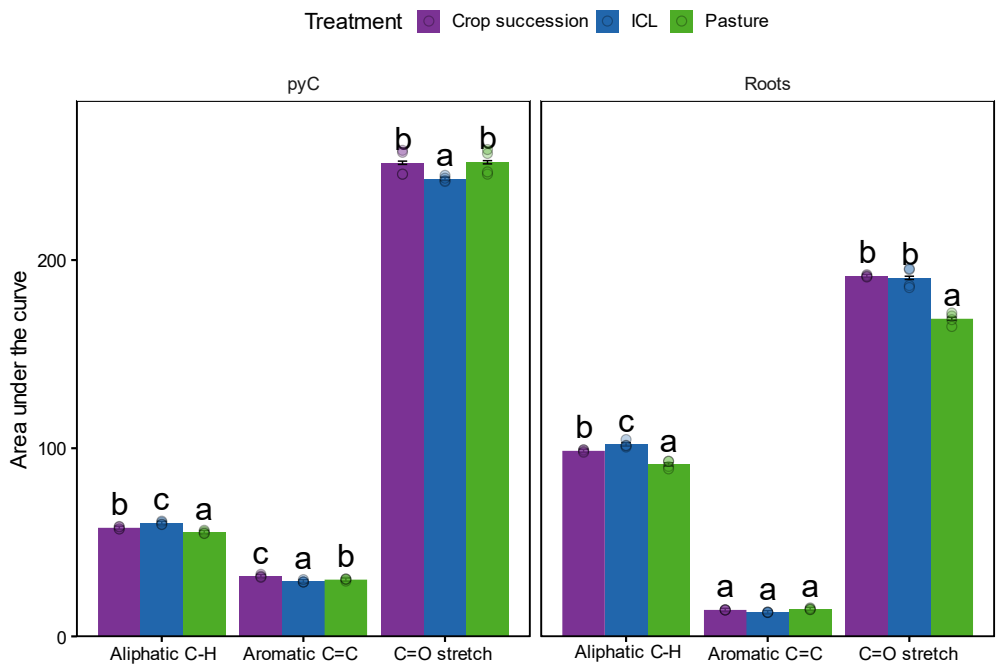

Fig. 4 The area under the curve of wavenumber range indicators for aliphatic (C-H stretch), aromatic (C=C) and carboxylic (C=O stretch) carbon in the two types of POM across the land uses. Shown are means and standard errors for the means, letters indicate significant differences among land uses within each ratio of each POM type ($p<0.05$).

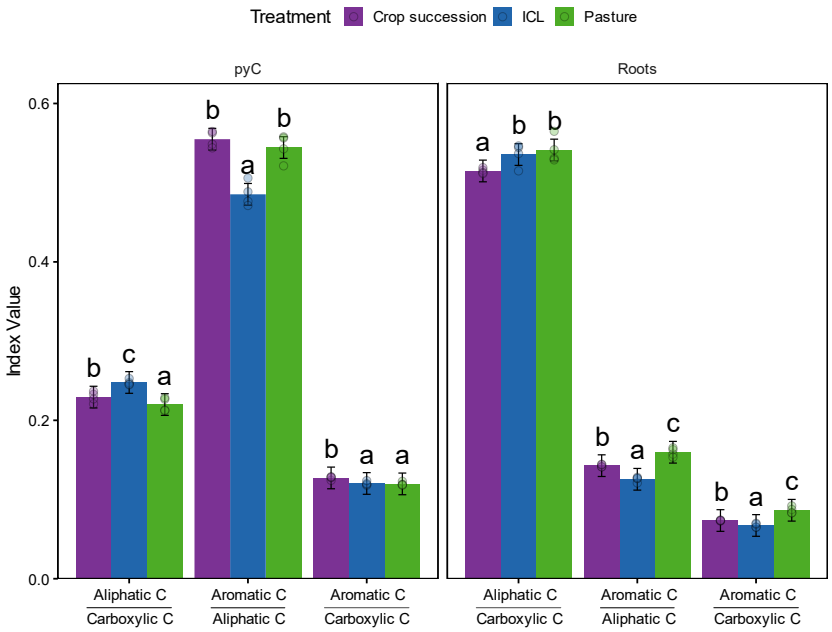

Fig. 5 Ratios of aliphatic, aromatic, and carboxylic carbon in the two types of POM from different land uses. Shown are means and standard errors for the means, letters indicate significant differences among land uses within each ratio of each POM type ($p<0.05$)

Discussion

Our hypothesis regarding the impact of land uses on the characteristics of the POM fragments of root origin was partially supported by the data. For instance, while Os concentrations of the roots did not differ among the three land use systems, differences in terms of aliphatic and carboxylic indicators were observed. However, the results did not support the other two hypotheses. Specifically, the three systems differed in terms of aliphatic, aromatic, and carboxylic indicators in the POM of pyrogenic origin, as well as in their ratios, with also a numeric tendency for differences in Os concentrations. Moreover, Os concentrations were significantly higher in POM of pyrogenic origin compared to that of root origin. These results highlight sorption capabilities of pyrogenic POM, and for the first time demonstrate an impact of long-term land use on composition and quantities of organic compounds that can be adsorbed by it.

Dual energy imaging of Os staining for visualization and quantification of SOC

Our improved procedure achieved higher staining efficiency than the past efforts of soil staining which also used gaseous source of Os. For example, Zheng et al. (2020) reported Os concentration of 1-5 mg cm^{-3} for POM fragments embedded in sand medium in an experimental setting comparable to this study, while here Os concentrations in the range of 18-39 mg cm^{-3} were achieved. Given the comparable experimental conditions and the carbon-rich nature of the organic materials, which offers abundant Os binding sites, we attribute our higher Os concentration values primarily to our newly developed staining protocol, i.e. Os saturation under vacuum.

Despite its potential for SOC exploration, Os staining is infrequently used due to complicated sample preparation and challenges in uniformity of Os delivery into intact soil samples, often resulting in noisy, low-contrast images. While formal method testing and comparison will be needed in the future, we surmise that vacuum facilitation of OsO_4 diffusion into porous media proposed here holds promise for ensuring better accessibility of SOC to the staining agent and for generating images with better contrast, especially important for future explorations of SOC within intact soil samples. Furthermore, the higher range of Os concentrations indicates a higher signal-to-noise ratio in our dual-beam synchrotron images, providing more reliable quantitative information on Os concentration per pixel than previous studies.

Differences in Os staining of pyC vs. root originated POM

As expected, the two types of POM markedly differed in their chemical compositions (Fig. 4 and 5). Higher aromatic and lower aliphatic groups in pyC compared to that in root POM (Fig. 4) were consistent with known highly aromatic nature of pyrogenic C sources generated by condensation reactions during biomass pyrolysis (Collard and Blin, 2014). The pyrolysis process enhances pyC aromaticity through cyclization of fatty hydrocarbon branch chains and condensable compounds, depleting olefinic bonds (Chen et al., 2024). This reduction in olefinic sites limits the availability of Os binding sites in these compounds, potentially reducing the effectiveness of staining. Indeed, consistent with this expectation Zheng et al. (2020) reported substantially lower Os staining for biochar fragments compared to root materials. However, our study generated contrasting results (Fig. 2), raising a question of why was the pyC POM not only did not exhibit less staining than root POM but also tended to accumulate higher Os concentrations? We suggest that the answer lies in the differences in the studied pyC materials. The pyC used by Zheng et al. (2020) consisted of biochar pyrolyzed in laboratory conditions shortly prior to the Os staining experiment, and it was not exposed to soil or any organic compounds. The pyC used in this study was procured directly from the soil. It was a relic of fires predating the establishment of the field experimental site (Nascimento et al., 2020; Roscoe et al., 2000), and all the time prior to our Os staining experiment the pyC POM was embedded within the soil, being in close contact with soil solutions, microorganisms, live and senescent plant roots, etc. Pyrogenic C is a strong geosorbent, highly porous with an extremely large reactive surface area, thus able to provide sorption sites for various organic molecules (Qi et al., 2017). We suggest that higher Os concentrations in pyC compared to root POM (Fig. 2) reflect the organic matter immobilized within it, rather than the inherent properties of pyC itself.

The effect of land use on pyC and root originated POM

The suggestion that Os staining results of this study reflected not only the properties of pyC itself but also of the organic material absorbed by it is supported by the observed differences in pyC Os staining among the land uses (Fig. 2). Since burning was not part of any studied land use practices at the experimental site, it is reasonable to assume that, initially, i.e., prior to 2011, pyC characteristics were uniform across the site. Therefore, the currently observed differences in Os concentrations, which followed the order of ICL > Pasture > Crop Succession, reflected the

influence of >10 years of contrasting land use on sorption of organic compounds by pyC (Fig. 4). In its chemical composition pyC from ICL stood out from those of Pasture and Crop Succession by its higher aliphatic and lower aromatic indicator values (Fig. 4 and 5). The lower aromatic to aliphatic C ratio in pyC POM of ICL suggests its enrichment with plant-derived aliphatic materials (e.g., cellulose-derived compounds and carbohydrates). However, it must be noted that the sizes of the differences between root and pyC POM fragments in terms of aliphatic and aromatic indicators greatly exceeded the differences between land uses for pyC (Fig. 4 and 5), yet without a subsequently greater Os staining. This observation suggests that FTIR spectroscopy might not be sufficiently sensitive to identify the specific functional groups and chemical compositions of roots vs. pyC POM fragments responsible for the interactions with OsO_4, emphasizing the importance of further studies.

Why does ICL, expected to fall between Crop Succession and Pasture, stand out in terms of Os staining and SOC chemical composition? We posit this is due to the recurrent intensive decomposition of large quantities of fresh organic matter inherent to ICL management. During every management cycle, ICL experiences two years of perennial grass growth during its pasture stage, likely leading to a significant build-up of fresh C inputs (Monteiro et al., 2024). Subsequent seeding of crops exposes these fresh inputs to intensive decomposition, and dissolved organic carbon from the resulting decomposition products comes into contact with tillage-dislodged pyC fragments and is adsorbed by them. This intensive input/decomposition cycle sets ICL apart from the two other land uses and, at least in part, explains the observed differences among them. Unlike ICL, Crop Succession lacks the build-up of new carbon due to rapid decomposition of relatively lower inputs of plant C, further accelerated by the annual seeding operations. In Pasture, the decomposition of continuously accumulating new C is minimal due to lack of soil disturbance. While further studies will be needed, these results point to a potentially important role of pyC in the storage and protection of newly plant-derived C in conservation management systems of tropical agriculture.

The FTIR spectral data analysis for roots (Fig. 4) showed notable differences among the three land uses in terms of their chemical composition. FTIR has previously been shown as a useful tool for distinguishing plant species (Legner et al., 2018). Aromatic C, usually an indicator of lignin in plant roots, did not differ across land uses, contrasting with the pyC aromatic C results.

Assuming roots are a major contributor to SOC, this suggests that plant lignin did not directly affect pyC composition or Os staining due to a lack of binding sites. The main differences in root spectral data were observed in aliphatic C (3000-2800 cm^{-1}), corresponding to lipids, wax, and fats (Legner et al., 2018). This aliphatic C pattern was reflected in the pyC results and, given its abundance of binding sites, is likely a primary contributor to the Os staining differences in pyC. The C=O stretch, commonly used as an indicator of protein in plant roots (Artz et al., 2008), was the lowest in the Pasture roots, aligning with the lower protein concentrations reported for palisade grass (Leite et al., 2021). Interestingly, there was no difference in C=O between the Crop succession and ICL. This likely reflects, in part, the ICL management practice, which aims to address increasing global animal protein demand by integrating both crops and forage systems as a sustainable pathway for land use in Brazilian agriculture (de Carvalho et al., 2019; Nascimento et al., 2021).

Our study demonstrates that land-use practices influence the chemical composition of pyC in tropical soils. The ICL system showed distinct characteristics in pyC composition compared to other land uses. The higher Os staining efficiency and lower aromatic-to-aliphatic carbon ratios observed in pyC under ICL suggest an enrichment of plant-derived aliphatic materials within pyC structures. These findings provide new insights into the potential role of pyC in interacting with newly decomposed plant carbon inputs in tropical agricultural soils. The results suggest that pyC POM may act as a storage medium for newly decomposed plant carbon inputs, offering new evidence of its potential role in SOC dynamics in tropical soils.

Further research is needed to fully understand and leverage these mechanisms. Future studies should focus on investigating the specific processes of SOC protection within pyC structures under different land-use systems, conducting long-term experiments to assess the stability and longevity of protected SOC in various agricultural systems, and exploring potential strategies to enhance pyC-mediated SOC storage in agricultural soils.

Acknowledgements

We thank Maxwell Oerther for help with laboratory analysis and Os staining. We gratefully acknowledge the support of the Brazilian Biorenewables National Laboratory (LNBR/CNPEM) and the Research Centre for Greenhouse Gas Innovation (RCGI), sponsored by FAPESP – São

Paulo Research Foundation (grants #2021/12914-3 and #2020/15230-5). Support for this research was also provided in part by the NSF DEB Program (Award # 1904267), and by the Great Lakes Bioenergy Research Center, U.S. Department of Energy. This research used resources of the Advanced Photon Source, a U.S. Department of Energy (DOE) Office of Science User Facility operated for the DOE Office of Science by Argonne National Laboratory under Contract No. DE-AC0206CH11357. We acknowledge the support of GeoSoilEnviroCARS (Sector 13), which is supported by the National Science Foundation - Earth Sciences (EAR-1128799), and the Department of Energy, Geosciences (DE-FG02-94ER14466).

References

Angst, G., Mueller, K.E., Castellano, M.J., Vogel, C., Wiesmeier, M., Mueller, C.W., 2023. Unlocking complex soil systems as carbon sinks: multi-pool management as the key. Nat Commun 14, 2967. https://doi.org/10.1038/s41467-023-38700-5

Arai, M., Uramoto, G.-I., Asano, M., Uematsu, K., Uesugi, K., Takeuchi, A., Morono, Y., Wagai, R., 2019. An improved method to identify osmium-stained organic matter within soil aggregate structure by electron microscopy and synchrotron X-ray micro-computed tomography. Soil and Tillage Research 191, 275–281. https://doi.org/10.1016/j.still.2019.04.010

Artz, R.R.E., Chapman, S.J., Jean Robertson, A.H., Potts, J.M., Laggoun-Défarge, F., Gogo, S., Comont, L., Disnar, J.-R., Francez, A.-J., 2008. FTIR spectroscopy can be used as a screening tool for organic matter quality in regenerating cutover peatlands. Soil Biology and Biochemistry 40, 515–527. https://doi.org/10.1016/j.soilbio.2007.09.019

Bates, D., Mächler, M., Bolker, B., Walker, S., 2015. Fitting Linear Mixed-Effects Models Using lme4. Journal of Statistical Software 67, 1–48. https://doi.org/10.18637/jss.v067.i01

Belazi, D., Solé-Domènech, S., Johansson, B., Schalling, M., Sjövall, P., 2009. Chemical analysis of osmium tetroxide staining in adipose tissue using imaging ToF-SIMS. Histochemistry & Cell Biology 132, 105–115. https://doi.org/10.1007/s00418-009-0587-z

Bieluczyk, W., Piccolo, M. de C., Pereira, M.G., Moraes, M.T. de, Soltangheisi, A., Bernardi, A.C. de C., Pezzopane, J.R.M., Oliveira, P.P.A., Moreira, M.Z., Camargo, P.B. de, Dias, C.T. dos S., Batista, I., Cherubin, M.R., 2020. Integrated farming systems influence soil organic matter dynamics in southeastern Brazil. Geoderma 371, 114368. https://doi.org/10.1016/j.geoderma.2020.114368

Bossio, D.A., Cook-Patton, S.C., Ellis, P.W., Fargione, J., Sanderman, J., Smith, P., Wood, S., Zomer, R.J., von Unger, M., Emmer, I.M., Griscom, B.W., 2020. The role of soil carbon in natural climate solutions. Nat Sustain 3, 391–398. https://doi.org/10.1038/s41893-020-0491-z

Brewer, K.M., Gaudin, A.C.M., 2020. Potential of crop-livestock integration to enhance carbon sequestration and agroecosystem functioning in semi-arid croplands. Soil Biology and Biochemistry 149, 107936. https://doi.org/10.1016/j.soilbio.2020.107936

Carvalho, J.L.N., Raucci, G.S., Cerri, C.E.P., Bernoux, M., Feigl, B.J., Wruck, F.J., Cerri, C.C., 2010. Impact of pasture, agriculture and crop-livestock systems on soil C stocks in Brazil. Soil and Tillage Research 110, 175–186. https://doi.org/10.1016/j.still.2010.07.011

Chen, J., Zhou, J., Zheng, W., Leng, S., Ai, Z., Zhang, W., Yang, Z., Yang, J., Xu, Z., Cao, J., Zhang, M., Leng, L., Li, H., 2024. A complete review on the oxygen-containing functional groups of biochar: Formation mechanisms, detection methods, engineering, and applications. Science of The Total Environment 946, 174081. https://doi.org/10.1016/j.scitotenv.2024.174081

Collard, F.-X., Blin, J., 2014. A review on pyrolysis of biomass constituents: Mechanisms and composition of the products obtained from the conversion of cellulose, hemicelluloses and lignin. Renewable and Sustainable Energy Reviews 38, 594–608. https://doi.org/10.1016/j.rser.2014.06.013

Collin, R.J., Griffith, W.P., 1974. Mechanism of Tissue Component Staining by Osmium Tetroxide. J Histochem Cytochem. 22, 992–993. https://doi.org/10.1177/22.10.992

Cotrufo, M.F., Ranalli, M.G., Haddix, M.L., Six, J., Lugato, E., 2019. Soil carbon storage informed by particulate and mineral-associated organic matter. Nat. Geosci. 12, 989–994. https://doi.org/10.1038/s41561-019-0484-6

de Carvalho, P., Domiciano, L.F., Mombach, M.A., do Nascimento, H.L.B., Cabral, L. da S., Sollenberger, L.E., Pereira, D.H., Pedreira, B.C., 2019. Forage and animal production on palisadegrass pastures growing in monoculture or as a component of integrated crop–livestock–forestry systems. Grass and Forage Science 74, 650–660. https://doi.org/10.1111/gfs.12448

Dor, M., Emmanuel, S., Brumfeld, V., Levy, G.J., Mishael, Y.G., 2019. Microstructural changes in soils induced by wetting and drying: Effects on atrazine mobility. Land Degradation and Development 30, 746–755. https://doi.org/10.1002/ldr.3256

Hubbell, J.H., Seltzer, S.M., 1995. Tables of x-ray mass attenuation coefficients and mass energy-absorption coefficients 1 keV to 20 meV for elements z = 1 to 92 and 48 additional substances of dosimetric interest (No. PB-95-220539/XAB; NISTIR-5632). National Inst. of Standards and Technology - PL, Gaithersburg, MD (United States). Ionizing Radiation Div.

Kögel-Knabner, I., Wiesmeier, M., Mayer, S., 2022. Mechanisms of soil organic carbon sequestration and implications for management, in: Rumpel, C. (Ed.), Burleigh Dodds Series in Agricultural Science. Burleigh Dodds Science Publishing, pp. 11–46. https://doi.org/10.19103/AS.2022.0106.02

Kravchenko, A.N., Guber, A.K., Razavi, B.S., Koestel, J., Quigley, M.Y., Robertson, G.P., Kuzyakov, Y., 2019. Microbial spatial footprint as a driver of soil carbon stabilization. Nature Communications 10, 3121. https://doi.org/10.1038/s41467-019-11057-4

Lal, R., 2004. Soil Carbon Sequestration Impacts on Global Climate Change and Food Security. Science 304, 1623–1627. https://doi.org/10.1126/science.1097396

Lê, S., Josse, J., Husson, F., 2008. FactoMineR: An R Package for Multivariate Analysis. Journal of Statistical Software 25, 1–18. https://doi.org/10.18637/jss.v025.i01

Legner, N., Meinen, C., Rauber, R., 2018. Root Differentiation of Agricultural Plant Cultivars and Proveniences Using FTIR Spectroscopy. Front. Plant Sci. 9. https://doi.org/10.3389/fpls.2018.00748

Lehmann, J., Kleber, M., 2015. The contentious nature of soil organic matter. Nature 528, 60–68. https://doi.org/10.1038/nature16069

Leite, R.G., Cardoso, A. da S., Fonseca, N.V.B., Silva, M.L.C., Tedeschi, L.O., Delevatti, L.M., Ruggieri, A.C., Reis, R.A., 2021. Effects of nitrogen fertilization on protein and

carbohydrate fractions of Marandu palisadegrass. Sci Rep 11, 14786. https://doi.org/10.1038/s41598-021-94098-4

Maenhout, P., De Neve, S., Wragg, J., Rawlins, B., De Pue, J., Van Hoorebeke, L., Cnudde, V., Sleutel, S., 2021. Chemical staining of particulate organic matter for improved contrast in soil X-ray μCT images. Sci Rep 11, 370. https://doi.org/10.1038/s41598-020-79681-5

Margenot, A.J., Parikh, S.J., Calderón, F.J., 2023. Fourier-transform infrared spectroscopy for soil organic matter analysis. Soil Science Society of America Journal n/a. https://doi.org/10.1002/saj2.20583

Monteiro, A., Barreto-Mendes, L., Fanchone, A., Morgavi, D.P., Pedreira, B.C., Magalhães, C.A.S., Abdalla, A.L., Eugène, M., 2024. Crop-livestock-forestry systems as a strategy for mitigating greenhouse gas emissions and enhancing the sustainability of forage-based livestock systems in the Amazon biome. Science of The Total Environment 906, 167396. https://doi.org/10.1016/j.scitotenv.2023.167396

Nascimento, A.F.D., Rodrigues, R.D.A.R., Silveira, J.G.D., Silva, J.J.N.D., Daniel, V.D.C., Segatto, E.R., 2020. Nitrous oxide emissions from a tropical Oxisol under monocultures and an integrated system in the Southern Amazon – Brazil. Revista Brasileira de Ciência do Solo 44, e0190123. https://doi.org/10.36783/18069657rbcs20190123

Nascimento, H.L.B., Pedreira, B.C., Sollenberger, L.E., Pereira, D.H., Magalhães, C.A.S., Chizzotti, F.H.M., 2021. Herbage accumulation, canopy structure and tiller morphology of marandu palisadegrass growing in open pasture and in silvopasture. Agroforest Syst 95, 339–352. https://doi.org/10.1007/s10457-020-00590-7

Parikh, S.J., Goyne, K.W., Margenot, A.J., Mukome, F.N.D., Calderón, F.J., 2014. Chapter One - Soil Chemical Insights Provided through Vibrational Spectroscopy, in: Sparks, D.L. (Ed.), Advances in Agronomy. Academic Press, pp. 1–148. https://doi.org/10.1016/B978-0-12-800132-5.00001-8

Peth, S., Chenu, C., Leblond, N., Mordhorst, A., Garnier, P., Nunan, N., Pot, V., Ogurreck, M., Beckmann, F., 2014. Localization of soil organic matter in soil aggregates using synchrotron-based X-ray microtomography. Soil Biology and Biochemistry 78, 189–194. https://doi.org/10.1016/j.soilbio.2014.07.024

Qi, F., Kuppusamy, S., Naidu, R., Bolan, N.S., Ok, Y.S., Lamb, D., Li, Y., Yu, L., Semple, K.T., Wang, H., 2017. Pyrogenic carbon and its role in contaminant immobilization in soils. Critical Reviews in Environmental Science and Technology 47, 795–876. https://doi.org/10.1080/10643389.2017.1328918

Rawlins, B.G., Wragg, J., Reinhard, C., Atwood, R.C., Houston, A., Lark, R.M., Rudolph, S., 2016. Three-dimensional soil organic matter distribution, accessibility and microbial respiration in macroaggregates using osmium staining and synchrotron X-ray computed tomography. SOIL 2, 659–671. https://doi.org/10.5194/soil-2-659-2016

Rivers, M.L., 2012. tomoRecon: High-speed tomography reconstruction on workstations using multi-threading. Proc. SPIE 8506, Developments in X-Ray Tomography VIII, San Diego, California, USA, p. 85060U. https://doi.org/10.1117/12.930022

Roscoe, R., Buurman, P., Velthorst, E.J., Pereira, J.A.A., 2000. Effects of fire on soil organic matter in a “cerrado sensu-stricto” from Southeast Brazil as revealed by changes in δ13C. Geoderma 95, 141–160. https://doi.org/10.1016/S0016-7061(99)00089-0

Sanderman, J., Hengl, T., Fiske, G.J., 2017. Soil carbon debt of 12,000 years of human land use. Proceedings of the National Academy of Sciences 114, 9575–9580. https://doi.org/10.1073/pnas.1706103114

Schlüter, S., Leuther, F., Albrecht, L., Hoeschen, C., Kilian, R., Surey, R., Mikutta, R., Kaiser, K., Mueller, C.W., Vogel, H.-J., 2022. Microscale carbon distribution around pores and particulate organic matter varies with soil moisture regime. Nat Commun 13, 2098. https://doi.org/10.1038/s41467-022-29605-w

Schlüter, S., Sheppard, A., Brown, K., Wildenschild, D., 2014. Image processing of multiphase images obtained via X-ray microtomography: A review. Water Resources Research 50, 3615–3639. https://doi.org/10.1002/2014WR015256

W. N. Venables, B. D. Ripley, 2002. Modern Applied Statistics with S, 4th ed, Fourth. ed. Springer, New York.

Yu, W., Huang, W., Weintraub-Leff, S.R., Hall, S.J., 2022. Where and why do particulate organic matter (POM) and mineral-associated organic matter (MAOM) differ among diverse soils? Soil Biology and Biochemistry 172, 108756. https://doi.org/10.1016/j.soilbio.2022.108756

Zheng, H., Kim, K., Kravchenko, A., Rivers, M., Guber, A., 2020. Testing Os Staining Approach for Visualizing Soil Organic Matter Patterns in Intact Samples via X-ray Dual-Energy Tomography Scanning. Environ. Sci. Technol. 54, 8980–8989. https://doi.org/10.1021/acs.est.0c01028

Supplementary

Table S1. ANOVA table for Os concentration in the two studied POM types of the three land uses. Shown are numerator (NDf) and denominator (DDf) degrees of freedom, F-values and p-values (bold when <0.05).

Source	NDf	DDf	F-value	p-value
Land Use	2	27	2.2	0.13
POM type	1	27	5.3	**0.029**
Land Use * POM type	3	27	1.0	0.37

Table S2. ANOVA table for FTIR spectral data in the two studied POM types of the three land uses. Shown are numerator (NDf) and denominator (DDf) degrees of freedom, F-values and p-values.

Source	NDf	DDf	F-value	p-value
Comparing differences in functional groups				
Functional group	2	43.2	93847.0	<.0001
Land Use	2	7.45	33.8	0.0002
POM type	1	4.91	1883.6	<.0001
Functional group*Land use	4	43.2	50.7	<.0001

Functional group*POM type	2	43.2	7492.9	<.0001
Land use: POM type	2	43.2	3.7	0.0322
Functional group*Land use*POM type	4	43.2	27.8	<.0001
Comparing differences in functional groups ratios				
Ratio	2	42.42	17774.7	<.0001
Land Use	2	8.38	31.5	0.0001
POM type	1	3.48	2950.6	<.0001
Ratio*Land use	4	42.42	51.8	<.0001
Ratio*POM type	2	42.42	10926.3	<.0001
Land use: POM type	2	42.42	80.8	<.0001
Ratio*Land use* POM type	4	42.42	5.5	0.0012